


## Article

# Loose Belt Fault Detection and Virtual Flow Meter Development Using Identified Data-driven Energy Model for Fan Systems

Gang Wang <sup>1,\*</sup> , Junke Wang <sup>2,3</sup>, Nurayn Tiarniyu <sup>2</sup>, Zufan Wang <sup>1,4</sup> and Li Song <sup>2</sup>

<sup>1</sup> Department of Civil and Architectural Engineering, University of Miami, Coral Gables, FL 33146, USA; zwang@tntstate.edu

<sup>2</sup> School of Aerospace and Mechanical Engineering, University of Oklahoma, Norman, OK 73019, USA; junke.wang@pnnl.gov (J.W.); ntiarniyu@ou.edu (N.T.); lsong@ou.edu (L.S.)

<sup>3</sup> Pacific Northwest National Laboratory, Richland, WA 99354, USA

<sup>4</sup> Department of Civil and Architectural Engineering, Tennessee State University, Nashville, TN 37209, USA

\* Correspondence: g.wang2@miami.edu; Tel.: +1-305-284-5555; Fax: 1-305-284-3492

**Abstract:** An energy model that correlates fan airflow, head, speed, and system power input is essential to detect device faults and optimize control strategies in fan systems. Since the application of variable-frequency drives (VFDs) makes the motor-efficiency data published by manufacturers inapplicable for VFD–motor–fan systems, the fan efficiency and drive (belt–motor–VFD) efficiency must be identified for each individual system to obtain accurate energy models. The objectives of this paper are to identify an energy model of existing VFD–motor–fan systems using available experimental data and demonstrate its applications in loose belt fault detection and virtual airflow meter development for optimal control. First, an approach is developed to identify the fan head, fan efficiency, and drive-efficiency curves using available fan head, speed, and system power input as well as temporarily measured airflow rate without measuring shaft power. Then, the energy model is identified for an existing VFD–motor–fan system. Finally, the identified model is applied to detect the slipped belt faults and develop the virtual airflow meter. The experiment results reveal that the developed approach can effectively obtain the energy model of VFD–motor–fan systems and the model can be applied to effectively detect slipped belt faults and accurately calculate the fan airflow rate.

**Keywords:** fans; drive systems; energy models; loose belt detection; virtual airflow meters



**Citation:** Wang, G.; Wang, J.; Tiarniyu, N.; Wang, Z.; Song, L. Loose Belt Fault Detection and Virtual Flow Meter Development Using Identified Data-driven Energy Model for Fan Systems. *Sustainability* **2023**, *15*, 12113. <https://doi.org/10.3390/su151612113>

Academic Editor: Shuhua Fang

Received: 7 June 2023

Revised: 2 August 2023

Accepted: 6 August 2023

Published: 8 August 2023



**Copyright:** © 2023 by the authors. Licensee MDPI, Basel, Switzerland. This article is an open access article distributed under the terms and conditions of the Creative Commons Attribution (CC BY) license (<https://creativecommons.org/licenses/by/4.0/>).

## 1. Introduction

Electric motor-driven fans in heating, ventilation, and air-conditioning (HVAC) systems account for about 7% of the primary energy usage in commercial buildings in the United States (U.S.) [1]. Since faulty or inefficient operations can lead to energy consumption 15% to 30% greater than optimal fault-free operation in HVAC systems [2], it is critical to detect device operation faults and optimize control strategies for the energy efficiency of electric motor-driven fan systems [3] using an energy model, which covers all the components in electric motor-driven fan systems.

### 1.1. Configuration of Fan Systems

Figure 1 shows a schematic of an electric motor-driven fan system, which includes all the basic components. Besides the fan, the motor is a key component, which functions as a bridge to connect the mechanical components to power grids and converts the electrical energy from power grids to the mechanical energy to the fan. The motor mechanical power output is also called the motor load and shaft power. Most of the electric motors in fan systems are alternating current (AC) three-phase induction motors and the AC induction motor speed is approximately proportional to the frequency ( $f$ ) of power supply [4].

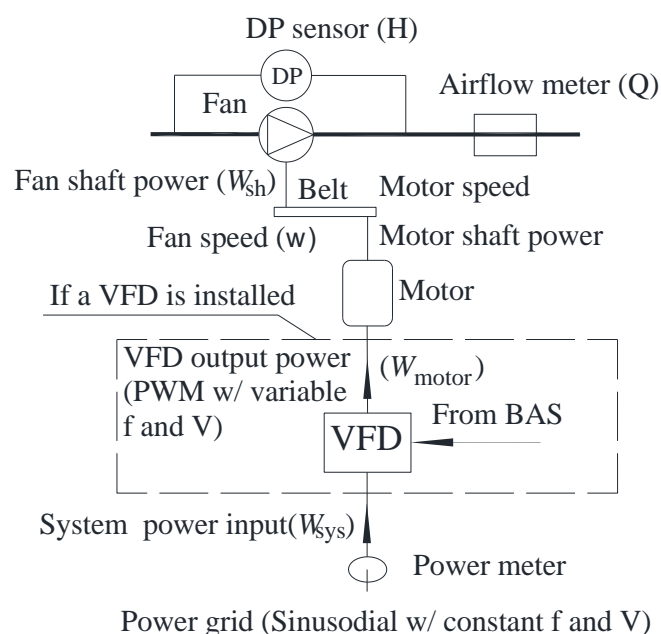


**Figure 1.** Schematic of a VFD–motor–fan system.

A belt typically connects the fan and motor to transfer the motor shaft power to the fan shaft power ( $W_{sh}$ ) to form the airflow ( $Q$ ) through the fan under the demanded fan head ( $H$ ) in most fan systems. The fan speed ( $\omega$ ) is proportional to the motor speed with a fixed-speed ratio, which is inversely proportional to the pulley diameter ratio between the fan and motor.

Seasonal changes in weather and daily schedules of occupants and plug loads make the space-cooling load as well as the required fan airflow more dynamic in commercial buildings. According to the affinity laws, the fan shaft power is proportional to the fan speed cubed and the fan airflow rate is proportional to the fan speed [5,6]. Thus, it is more energy efficient to reduce the fan speed than to close dampers at partial load conditions. Therefore, AC induction motors are often paired with variable-frequency drives (VFDs) to significantly reduce the fan system power by adjusting VFD output frequency ( $f$ ) under partial load conditions [6]. So, the fan speed ( $\omega$ ), motor speed, and VFD output frequency ( $f$ ) are proportional and the relative fan speed, motor speed, and VFD output frequency, with respect to the full design speeds and the rated power frequency, are the same and exchangeable in this paper.

Thus, with the application of a VFD, a fan system becomes a VFD–motor–fan system that comprises a fan and its drive system, including a belt, a motor, and a VFD. The energy model needs to be developed based on the fan and its drive system.

### 1.2. Energy Model Review

As a mechanical component, the energy model of a fan is relatively straightforward and, basically, defined by the fan head–airflow curve and the fan shaft power–airflow curve at a full design speed. Then, the affinity laws are applied to obtain the fan head and shaft power curves at any speed other than the full design speed [5,6]. The fan efficiency is defined as the ratio of the product of the airflow rate and head to the fan shaft power. Alternatively, the fan shaft power–head curve can be obtained using the fan head–airflow curve and the fan shaft power–airflow curve. As a result, only two of the four fan curves are independent, and the fan energy model can be determined by any two of these four fan curves. In this paper, the fan head–airflow curve and the fan-efficiency curve are identified first and are applied to obtain the other two curves.

On the other hand, the energy model of a drive system is simply defined by the drive efficiency, the ratio of the fan shaft power ( $W_{sh}$ ) to the system power input ( $W_{sys}$ ), which is

a product of the efficiency of a belt, a motor, and a VFD. The belt efficiency is defined as the ratio of the fan shaft power to the motor shaft power, the motor efficiency is defined as the ratio of the motor shaft power to the motor power input ( $W_{motor}$ ), and the VFD efficiency is defined as the ratio of the system power input to the VFD to the VFD output power to the motor, which is also the motor power input. Among them, the motor and VFD are electrical components and, traditionally, motor and VFD efficiency curves are not well understood by HVAC engineers. As a result, the motor and VFD efficiencies are often ignored or simplified in the energy model of VFD–motor–fan systems.

For example, Qiu et al. [7], Mollios et al. [8], Kong et al. [9], Wijaya et al. [10], Afram et al. [11], and Ji et al. [12] completely ignored VFD and motor efficiencies, V.K. Shankar et al. [13], Yiqun Pan et al. [14], Chilundo et al. [15], and R. Saidur et al. [16,17] ignored VFD efficiency and utilise a simplified motor efficiency which is treated as a constant, and Viholainen et al. [18] and Wang et al. [19] treated both VFD and motor efficiencies as constant. With these simplifications, the electrical power input to fan systems can be simply treated to be proportional to the fan speed cubed, just like the fan shaft power. However, the inaccurate motor and VFD efficiency model can result in an error of calculated system power input.

Induction motors are initially designed to be powered by power grids, which provide pure sinusoidal power with constant rated voltage and frequency. As a result, the motor efficiency is only impacted by the motor shaft power. IEEE Standard 112 is used for testing the efficiency of induction motors in the U.S. [20]. The standard clearly states the motor-efficiency testing condition is that the power supply should be a sinusoidal waveform with constant rated voltage and frequency. Currently, most motor manufacturers provide motor-efficiency data at various motor loads under this standard testing condition [21]. Naturally, these available data are applied to regress the motor-efficiency curves for VFD–motor–fan systems. For example, several U.S. DOE-sponsored energy-simulation programs, such as EnergyPlus [22], fan-system assessment tool (FSAT) [23], and pumping-system assessment tool (PSAT) [24], also use the motor-efficiency curves which were directly regressed based on the efficiency data published by motor manufacturers.

In fact, the application of VFDs renders motor efficiency more complicated. When a motor is powered by a VFD, the VFD output power to the motor is the pulse width modulation (PWM) power at variable voltage and frequency, which is significantly different from the sinusoidal power in power grids and renders the motor-efficiency data published by manufacturers inapplicable for VFD–motor–fan systems [6]. Both the motor equivalent circuit theory [4,25] and available experimental data [26–29] revealed that the motor efficiency associated with VFDs is a function of not only motor shaft power but also VFD output frequency and voltage. In general, the PWM power slightly degrades motor efficiency due to harmonics while the variable voltage significantly upgrades motor efficiency by matching motor power input with motor shaft power [30]. Ignoring the PWM and variable voltage impacts by EnergyPlus can under-estimate the motor efficiency by 10–25% in a frequency range between 30 and 40 Hz, as shown in Figure 2 [30].

VFDs, as electrical devices, also consume energy by the semiconductor components residing in control circuits, which can be reflected by the VFD efficiency. The U.S. Department of Energy [31] presented the VFD efficiency data as a function of the VFD output power, which is also the motor power input. Meanwhile, some VFD manufacturers provided VFD efficiency data as a function of both the VFD output power and frequency [32].

Overall, the drive efficiency is theoretically impacted by three influencing factors—the fan shaft power, VFD output voltage, and frequency. Thus, it is hard to regress the complicated drive-efficiency function with three influencing factors. On the other hand, the three factors are correlated in a VFD–motor–fan system. Most VFDs on the market provide different voltage–frequency (V/f) ratio controls. The squared ratio controls the voltage to be proportional to the square of the frequency, which is recommended for centrifugal fans. Moreover, the motor load is approximately proportional to the cube of the motor speed, which is proportional to the VFD output frequency, for centrifugal fans.

Thus, the drive efficiency can be simplified as a function of the fan speed or VFD output frequency by consolidating three influencing factors.

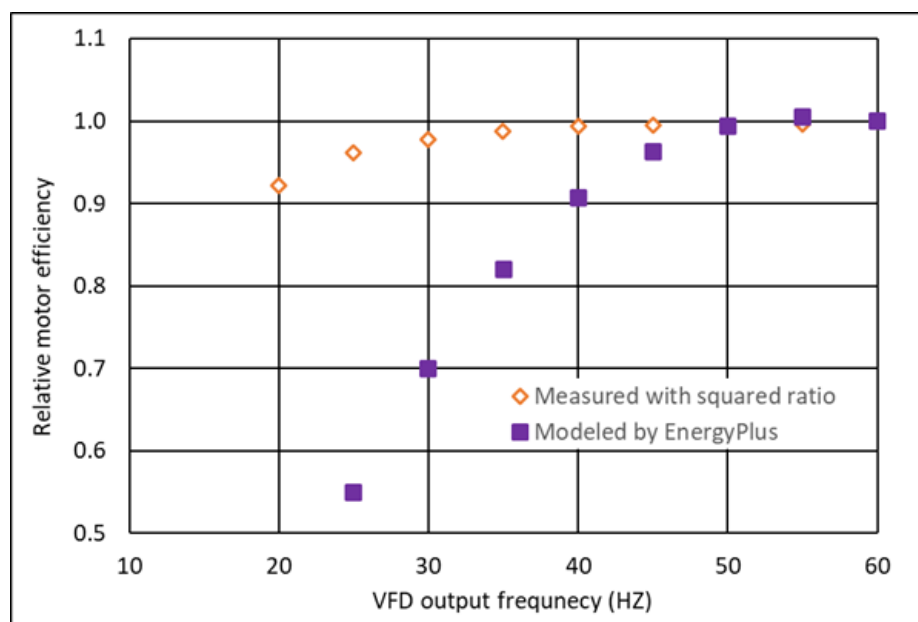


**Figure 2.** Comparison of measured and modeled motor efficiencies in a fan system.

Due to the lack of available motor-efficiency data for VFD–motor–fan systems, the drive-efficiency curve along with the fan head and efficiency curves need to be identified through experiments for existing fan systems individually.

### 1.3. Challenges to Identify the Energy Model

The available operation parameters in a VFD–motor–fan system determine the identification approach of fan system energy models. In general, the VFD output frequency ( $f$ ) can be obtained from the VFD, the fan head ( $H$ ) can be measured by a differential pressure (DP) transducer, the system power input to the VFD ( $W_{sys}$ ) can be measured by a conventional power meter, and the airflow rate ( $Q$ ) can be measured by multiple air velocity probes traversing supply air ducts, as shown in Figure 1. On the other hand, the fan shaft power cannot be measured in existing systems since it is impossible to install torque sensors. The fan head-airflow can be readily identified with the available fan airflow, head, and speed. However, the challenge is to identify the motor efficiency and fan efficiency simultaneously without measuring the fan shaft power.

Machine learning can be applied to identify the fan system model with comprehensive algorithms. For example, Mei and Levermore applied an artificial neural network to model the non-linear fan head-airflow curve [33].

On the other hand, since fan efficiency and drive efficiency have a clear correlation, a simple algorithm will be developed in this paper.

### 1.4. Application of Energy Models in Fan Systems

Belt wear is one common fault in fan systems which can lead to efficiency and performance problems. As belt slippage increases, motors cannot translate required shaft power to fans through a slipped belt [6] and fans cannot deliver airflow required by the terminal boxes and result in indoor comfort issues. The investigation conducted by Wang et al. [29] shows that the loose belts are significant at high fan speed and insignificant at lower fan speed.

The loose belt fault is traditionally detected by measuring fan airflow, head, and power to calculate the actual fan efficiency and compare it with fault-free efficiency [29,34]. However, the airflow meter is typically not installed at AHUs and traditional loose belt



detection approaches have this limitation. In fact, when the belt is loose, the actual head will offset from the fault-free head, which is determined using the head-shaft power curve in the energy model. Thus, the loose belt fault can be detected using measurable fan head, speed, and power without the airflow measurement along with the identified energy model.

On the other hand, optimal controls, such as duct static pressure control [35], building pressure control [36], outdoor air control [36,37], and cooling demand control [38], all require the fan airflow measurement at air handling units (AHUs). Unfortunately, physical airflow meters are not typically installed at AHUs due to space and cost limitations. When a fan system operates under a fault-free condition, the fan airflow can be virtually calculated based on other measurable variables, such as the fan head, speed, and system power input, using the fan and drive efficiencies in the identified energy model. Thus, virtual fan airflow meters are recommended to overcome the limitations of physical flow meters.

Therefore, a comprehensive energy model, which correlates the fan airflow rate, head, speed, and system power input, is required to detect loose belt faults and develop virtual fan airflow meters.

### 1.5. Objectives

In summary, the fan energy model can be defined by the fan head-airflow curve and the fan-efficiency curve, while the drive system model can be defined by the drive efficiency–fan speed curve. Thus, the fan head, speed, airflow rate, shaft power, and system power input are involved in modeling VFD–motor–fan systems. Among them, the fan speed, fan head, system power input, and fan airflow rate are measurable in existing VFD–motor–fan systems. The major challenge is that the fan shaft power is difficult to measure. Consequently, the direct identification of the fan-efficiency curve and drive-efficiency curve is not realistic.

The objectives of this paper are to identify an energy model of existing VFD–motor–fan systems using available experimental data and demonstrate its applications in loose belt fault detection and virtual airflow meter development for optimal control. First, an identification approach is developed to identify the fan head and efficiency curves and drive-efficiency curves using available fan head, speed, and system power input as well as temporarily measured airflow rate. Then, the energy model is identified for an existing VFD–motor–fan system with a design airflow of 1200 L/s using the developed approach. Finally, the identified model is applied to detect the slipped belt faults and to develop the virtual airflow meter for potential optimal AHU control with the measurements of fan head, speed, and system power input.

## 2. Theory and Identification Approach

In this section, two basic fan-performance curves, including the fan head-airflow curve and the fan shaft power-airflow curve at the full design speed, are defined and the resultant fan head-shaft power curve and fan-efficiency curve are derived. Then the fan performance curves at variable speeds and speed-independent fan-efficiency curves are derived using the affinity laws. Next, the speed-dependent drive-efficiency curve is defined based on the previous consolidation discussion. Finally, an identification approach is developed to identify the fan-efficiency curve and the drive-efficiency curve without measuring fan shaft power.

### 2.1. Fan Performance Curves at the Full Design Speed

The energy model of a fan is, basically, defined by two curves, which are the fan head-airflow rate curve and shaft power-airflow rate curve, at the full design speed. Both curves can be expressed as a function of the fan airflow rate:

$$H_d = f_{H-Q}(Q_d) \quad (1)$$

$$W_{sh,d} = f_{W-Q}(Q_d) \quad (2)$$

where  $H_d$ ,  $W_{sh,d}$ , and  $Q_d$  are the fan head, shaft power, and airflow rate at the full design speed, respectively.

Furthermore, the fan head-shaft power curve and fan-efficiency curve can be derived based on these two basic performance curves.

$$H_d = f_{H-W}(W_{sh,d}) \quad (3)$$

$$\eta_{fan,d} = \frac{Q_d \cdot H_d}{W_{sh,d}} = f_{\eta-Q}(Q_d) \quad (4)$$

## 2.2. Affinity Laws

The affinity laws state that the fan airflow rate is proportional to the fan speed, the fan head is proportional to the fan speed squared, and the fan shaft power is proportional to the fan speed cubed. If the fan speed ( $\omega$ ) is written in a relative value with respect to the full design speed, the affinity laws can be expressed as:

$$Q_d = \frac{Q}{\omega} \quad (5a)$$

$$H_d = \frac{H}{\omega^2} \quad (5b)$$

$$W_{sh,d} = \frac{W_{sh}}{\omega^3} \quad (5c)$$

First, the affinity laws are applied to transfer the fan-performance curves at the full design speed ( $\omega = 1$ ) to the fan-performance curves at any speed,  $\omega$ , and vice versa.

$$H = \omega^2 f_{H-Q}\left(\frac{Q}{\omega}\right) \quad (6)$$

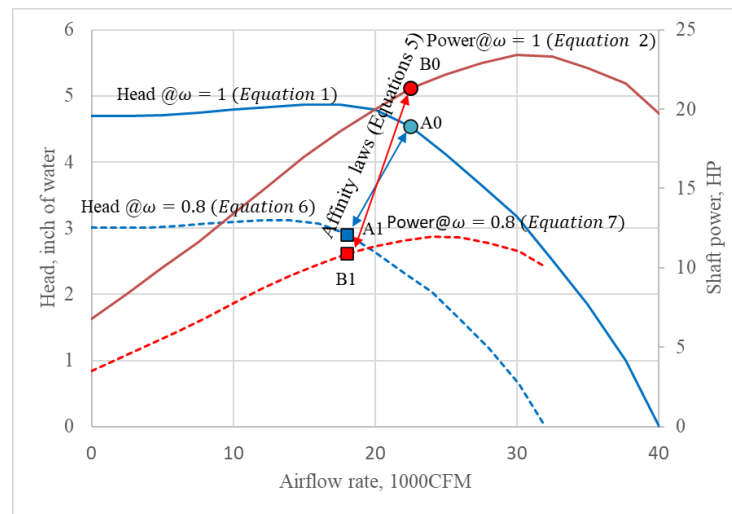
$$W_{sh} = \omega^3 f_{W-Q}\left(\frac{Q}{\omega}\right) \quad (7)$$

$$H = \omega^2 f_{H-W}\left(\frac{W_{sh}}{\omega^3}\right) \quad (8)$$

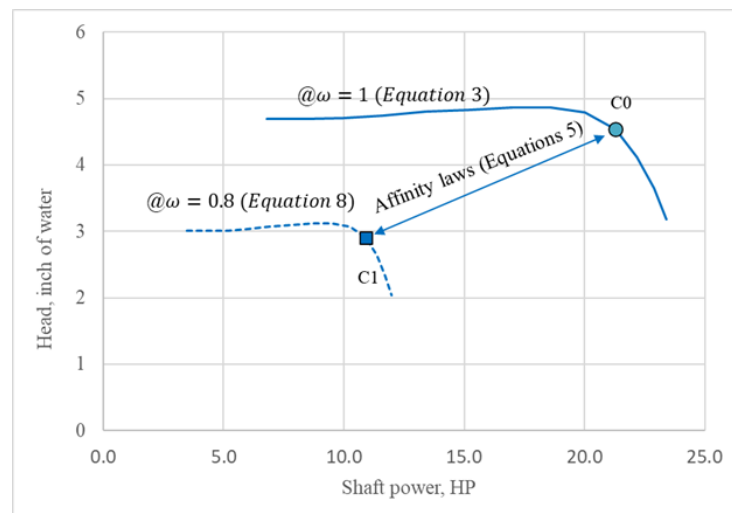
$$\eta_{fan,d} = f_{\eta-Q}\left(\frac{Q}{\omega}\right) \quad (9)$$

Figure 3a compares the fan head-airflow curves and the shaft power-airflow curves, Figure 3b compares the fan head-shaft power curves and Figure 3c compares the fan-efficiency curves at the design full speed ( $\omega = 1$ ) and a partial speed ( $\omega = 0.8$ ) for a typical centrifugal fan. In Figure 3, the fan curves at the design full speed are defined by Equations (1)–(4), the converted fan curves at the 80% speed are defined by Equations (6)–(9), and the conversion between the points, A0, B0, C0, and D0, at the design full speed, and their similar points, A1, B1, C1, and D1, at the 80% speed, is conducted using Equations (5a)–(5b).

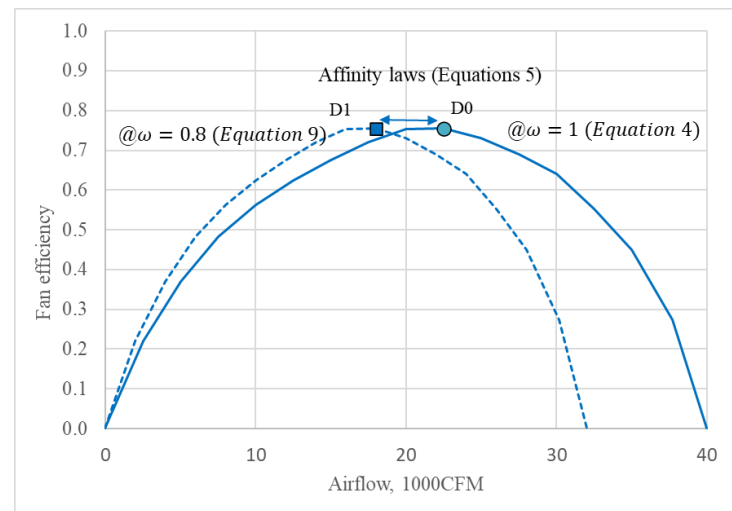
Equation (6) will be applied to directly identify the basic fan head-airflow curve at the full design speed using fan airflow ( $Q$ ) and head ( $H$ ) at actual fan speed ( $\omega \leq 1$ ), Equation (7) will be applied to create the basic fan shaft power-airflow curve at the full design speed with the identified drive efficiency while Equation (8) will be applied to detect the loose belt faults using fan head, shaft power at any speed. It is also noted that the fan efficiency in Equation (9) is a function dependent of the fan speed.



(a) Fan head-airflow curve and fan shaft power-airflow curves



(b) Fan head-shaft power curve



(c) Fan-efficiency-airflow curve

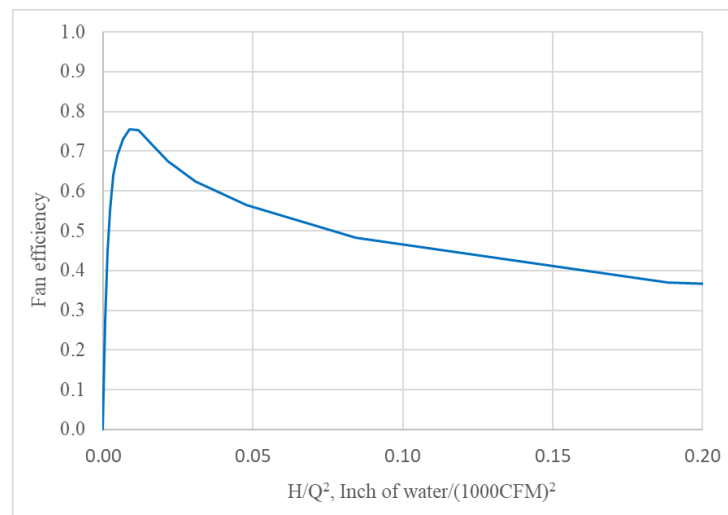
**Figure 3.** Fan curve conversion between the design full speed and a partial speed.

Second, according to the affinity laws, the sufficient and necessary conditions of the similarity are that the points have the same value of the ratio of the fan head to airflow squared, the ratio of the fan shaft power to the airflow cubed, and the ratio of fan shaft power squared to the fan head cubed. Consequently, the similar points also have the same ratio of the product of the fan airflow and head to the fan shaft power, or the same fan efficiency. Thus, the affinity laws are applied to obtain the fan-efficiency functions independent of the fan speed in Equations (10) and (11).

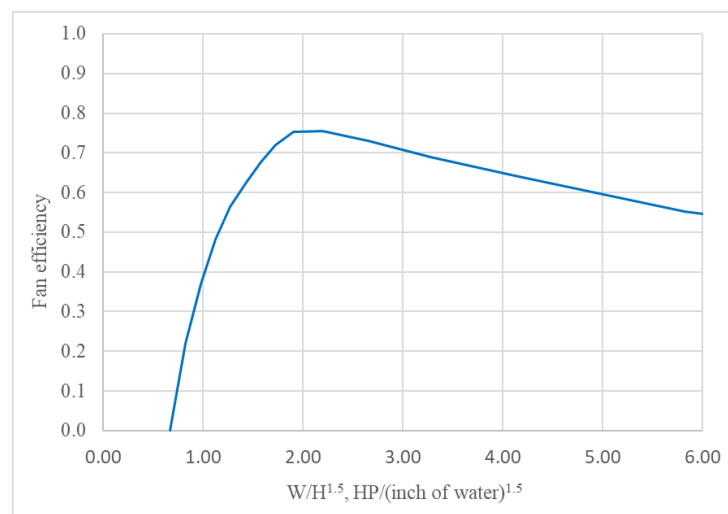
$$\eta_{fan} = \frac{Q \cdot H}{W_{sh}} = f_{H\&Q} \left( \frac{H}{Q^2} \right) \quad (10)$$

$$\eta_{fan} = \frac{Q \cdot H}{W_{sh}} = f_{W\&H} \left( \frac{W_{sh}}{H^{1.5}} \right) \quad (11)$$

Figure 4a shows the fan efficiency versus ratio of fan head to airflow squared curve and Figure 4b shows the fan efficiency versus the ratio of the shaft power to fan head to the power of 1.5 curve for the same fan defined in Figure 3.



(a) Efficiency versus the ratio of fan head to airflow squared



(b) Efficiency versus the ratio of fan shaft power to fan head to the power of 1.5

**Figure 4.** Speed-independent fan-efficiency curves.

The fan efficiency in Equation (10) plays a key role in separating the drive efficiency and fan efficiencies without measuring the fan shaft power for the model identification. The fan efficiency in Equation (11) plays a key role in detecting the loose belt faults and develop the virtual fan airflow meter where the fan airflow is not available.

### 2.3. Drive Efficiency and System Efficiency

After the consolidation, the drive efficiency can be expressed as a function of the fan speed.

$$\eta_{drive} = \frac{W_{sh}}{W_{sys}} = f_{drive}(\omega) \quad (12)$$

During the identification process, the fan shaft power is not available. As result, the fan efficiency that correlates the available fan airflow and head to the unknown fan shaft power and the drive efficiency that correlates the available system power input to the unknown fan shaft power cannot be directly identified.

The system efficiency ( $\eta_{sys}$ ), is defined as the ratio of the product of the flow rate and head to the system power input and is the product of the fan efficiency and drive efficiency.

$$\eta_{sys} = \frac{Q \cdot H}{W_{sys}} = \eta_{drive} \cdot \eta_{fan} = f_{drive}(\omega) f_{H\&Q}\left(\frac{H}{Q^2}\right) \quad (13)$$

First, with the available fan airflow rate, head and system power input, the system efficiency is always available. Second, two uncorrelated efficiency functions, the speed-dependent drive-efficiency function, and the speed-independent fan-efficiency function, can be applied to separate the fan efficiency and drive efficiency from the available system efficiency.

### 2.4. Identification Approach

Figure 5 shows the flow chart of the four-step identification approach.

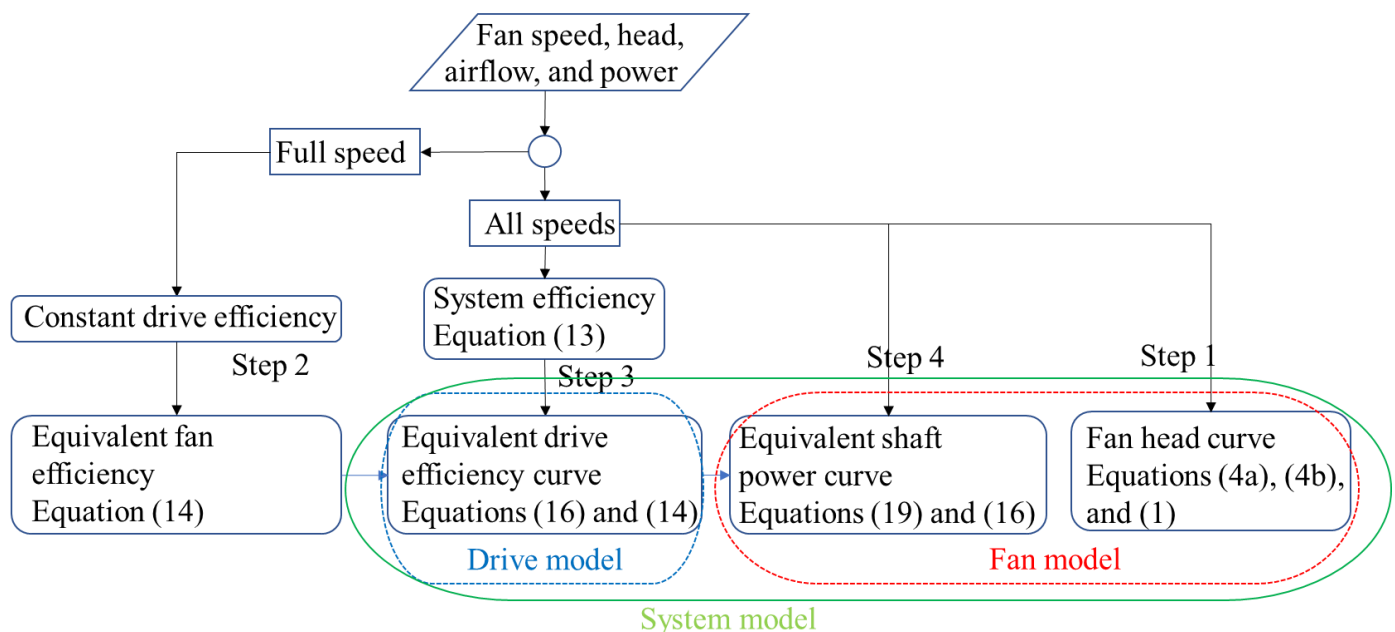


Figure 5. Identification flow chart.

#### Step 1: Fan head curve at the full design speed

Since the fan head-airflow curve is independent of the unmeasurable shaft power, the fan head curve at the full design speed, defined by Equation (1), can always be directly obtained by measuring the fan speed, head, and airflow rate at all the speeds and applying



the affinity laws, defined by Equations (5a) and (5b). The intention to use the data at all the speeds is to make a fan head curve at the full design speed with a wider airflow range.

### Step 2: Fan-efficiency function

Since the fan shaft power is not measurable, it must be converted from the measured system power input using the drive efficiency. The fan efficiency needs to be determined first and, then, applied to separate the drive efficiency from the system efficiency, which can be directly obtained without measuring the fan shaft power. If the fan efficiency is expressed as a function of the ratio of the fan head to the airflow rate squared, as shown in Equation (10), the fan efficiency is independent of the fan speed. Consequently, the fan-efficiency curve can be identified using the performance data at the full design speed ( $\omega = 1$ ) only.

Since the drive efficiency is a function of the fan speed, the drive efficiency at the full design speed is an unknown constant. Thus, the system efficiency at the full design speed becomes the product of the fan efficiency and the unknown constant drive efficiency and is defined as the equivalent fan efficiency ( $\eta_{fan,e}$ ) by Equation (14). The equivalent fan-efficiency curve can be regressed using the measured fan airflow rate, head, and system power input at the full design speed ( $\omega = 1$ ):

$$\eta_{sys@ \omega=1} = \frac{Q \cdot H}{W_{sys}} = \eta_{drive}(\omega = 1) \cdot \eta_{fan} \left( \frac{H}{Q^2} \right) = \eta_{fan,e} \left( \frac{H}{Q^2} \right) \quad (14)$$

### Step 3: Drive-efficiency function

The equivalent fan-efficiency curve,  $\eta_{fan,e} \left( \frac{H}{Q^2} \right)$ , is then applied to obtain the drive efficiency versus fan speed curve by using the performance data at all fan speeds.

$$\eta_{drive}(\omega) = \frac{Q \cdot H}{\eta_{fan} \left( \frac{H}{Q^2} \right) W_{sys}} = \frac{Q \cdot H \cdot \eta_{drive}(\omega = 1)}{\eta_{fan,e} \left( \frac{H}{Q^2} \right) W_{sys}} \quad (15)$$

To consolidate the unknown constant drive efficiency at the full design speed in Equation (15), the equivalent drive efficiency is defined as the ratio of the drive efficiency at any fan speed to the drive efficiency at the full design speed. Thus, the equivalent drive-efficiency curve ( $\eta_{drive,e}$ ) can be regressed using the measured fan airflow rate, head, and system power input at all fan speeds as well as the identified equivalent fan-efficiency curve, Equation (14) in Step 2.

$$\eta_{drive,e}(\omega) = \frac{\eta_{drive}(\omega)}{\eta_{drive}(\omega = 1)} = \frac{Q \cdot H}{\eta_{fan,e} \left( \frac{H}{Q^2} \right) W_{sys}} \quad (16)$$

According to Equations (14) and (16), the equivalent fan efficiency and equivalent drive efficiency can be identified without measuring the fan shaft power. More importantly, even though they are not true fan efficiency and true drive efficiency, the product of them is the true system efficiency, which can correlate the measurable fan head and airflow rate to the measurable system power input.

$$\eta_{fan,e} \left( \frac{H}{Q^2} \right) \eta_{drive,e}(\omega) = \eta_{sys} = \frac{Q \cdot H}{W_{sys}} \quad (17)$$

As a result, the challenge with unmeasurable fan shaft power is solved by:

- Using the available system efficiency, defined by Equation (13);
- Defining the equivalent fan efficiency and equivalent drive efficiency using Equations (14) and (16);
- Expressing them by two uncorrelated functions in Equation (17), the equivalent fan-efficiency function of the ratio of fan head to airflow rate squared and the equivalent

drive-efficiency function of the fan speed, to separate the equivalent fan efficiency and equivalent drive efficiency from the system efficiency.

#### **Step 4: Fan shaft power curve at the full design speed**

According to Equation (13), the fan shaft power ( $W_{sh}$ ) at all fan speeds can be calculated from the measured system power input ( $W_{sys}$ ) along with the drive-efficiency curve ( $\eta_{drive}$ ), which is the product of the equivalent drive efficiency ( $\eta_{drive,e}$ ) and the unknown constant drive efficiency at the full design speed:

$$W_{sh} = W_{sys}\eta_{drive}(\omega) = W_{sys}\eta_{drive,e}(\omega)\eta_{drive}(\omega = 1) \quad (18)$$

To consolidate the unknown drive efficiency at the full design speed in Equation (18), the equivalent fan shaft power is defined as the ratio of the fan shaft power to the drive efficiency at the full design speed.

$$W_{sh,e} = W_{sh}/\eta_{drive}(\omega = 1) = W_{sys}\eta_{drive,e}(\omega) \quad (19)$$

Two equivalent shaft power-related curves, including an equivalent fan shaft power-airflow curve and a fan head-equivalent shaft power curve, at the full design speed can be created with the calculated equivalent fan shaft power, and measured airflow rate and fan head using affinity laws.

Note that Equation (13) that correlates the measured fan head, airflow, and system power inputs is still valid with equivalent fan efficiency, equivalent drive efficiency, and equivalent shaft power.

### **3. Model Identification Demonstration**

#### **3.1. Test System**

The experiments were conducted on a VFD–motor–fan system in an AHU serving a portion of an institution building. The total serving area is about 214 m<sup>2</sup> (2300 ft<sup>2</sup>) and the total cooling capacity of the AHU is 28 kW (8 ton). The supply fan with a design flow rate of 1200 L/s (2500 CFM) is a forward curve blade centrifugal fan and is equipped with a 2.2 kW (3 hp) motor powered by a VFD which connects the fan through a cogged belt.

The fan speed is modulated by the VFD through the building automation system (BAS) to maintain the supply air duct static pressure at its setpoint, normally 248 Pa (1.0 inch of water). The squared ratio voltage control was set at the VFD. During the experiments, the supply fan was almost operated under routine control sequences except a few control overrides for other research projects, which made the operation more dynamic. During a period when the fan is speeding up, the additional system power input is required to accelerate the air movement and vice versa while the increased fan airflow and head are recorded with a time delay due to the sensor time constant.

An air DP sensor was installed across the supply fan to measure the fan head. A factory-mounted and pre-piped duct-mounted airflow duct airflow station (with accuracy within 2% of the actual flow rate) was installed on the 356 mm by 559 mm (14 inch by 22 inch) supply duct. It is noted that for AHUs without a physical airflow meter, multiple air velocity probes need to be temporarily installed to traverse the supply air duct to measure the airflow rate.

Moreover, one VFD analog output channel was assigned to the motor power input using a MODBUS connection, a popular communication protocol, and a conventional power meter was installed upstream of the VFD to measure the system power input. Since the VFD analog output channel only has one decimal place, the motor power input reading jumps up and down among several discrete readings from 0.5 to 1.3 kW for this small-sized 2.2 kW (3 hp) motor. As a result, the motor power input reading from the VFD cannot be used to identify the energy model. The case with accurate motor power input reading from VFDs for large-sized motors will be discussed at the end of the paper.

A computer, serving as a server, was connected to the experimental system through a universal control network for control, real-time monitoring, data collection, and storage purposes. The collected data include the fan speed command in addition to the fan airflow, fan head, and system power input with a sampling time of one minute, which is the shortest sampling for this control system.

The configuration of the test system is shown in Figure 6.

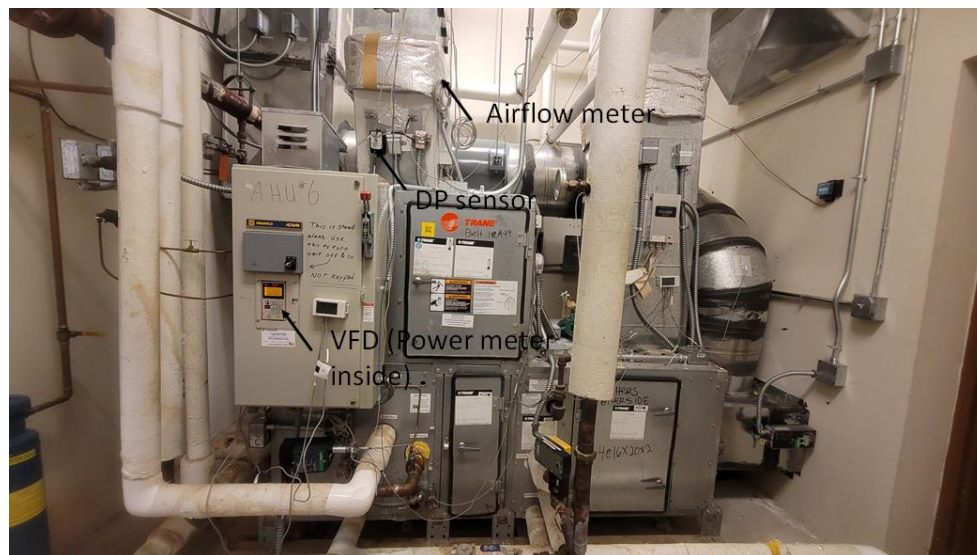


**Figure 6.** Configuration of the studied AHU.

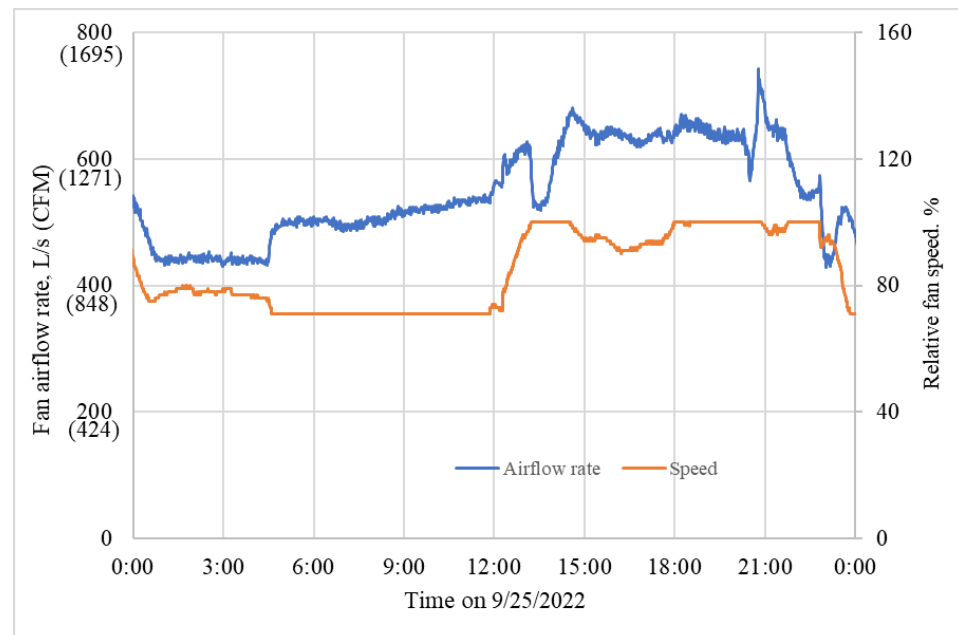
### 3.2. Performance Data Collection

The performance data from 11 September to 17 October 2022 are applied to identify the VFD–motor–fan system model. Figure 7a shows the measured fan airflow rate and percentage speed, while Figure 7b shows the measured fan head and system power input over a one-day period. As observed, the fan airflow, speed, and head measurements are relatively stable, while the power measurement (orange curve) has significant oscillations due to the VFD PWM power output. It is important to process the power data before using them to identify the VFD–motor–fan system model. Two data processing measures were conducted to eliminate the oscillations in this study, i.e., using the 10-sample average (yellow) and median (gray) values. The two manipulated power values are also shown in Figure 7b. Since the median power input shows a better match with the fan speed, the 10-sample median power value was applied afterward. To further improve the accuracy of the power measurement, it is recommended to record the system power input with a shorter sampling time, such as 5 s, using a data logger outside the control system, to accurately catch the system dynamics.

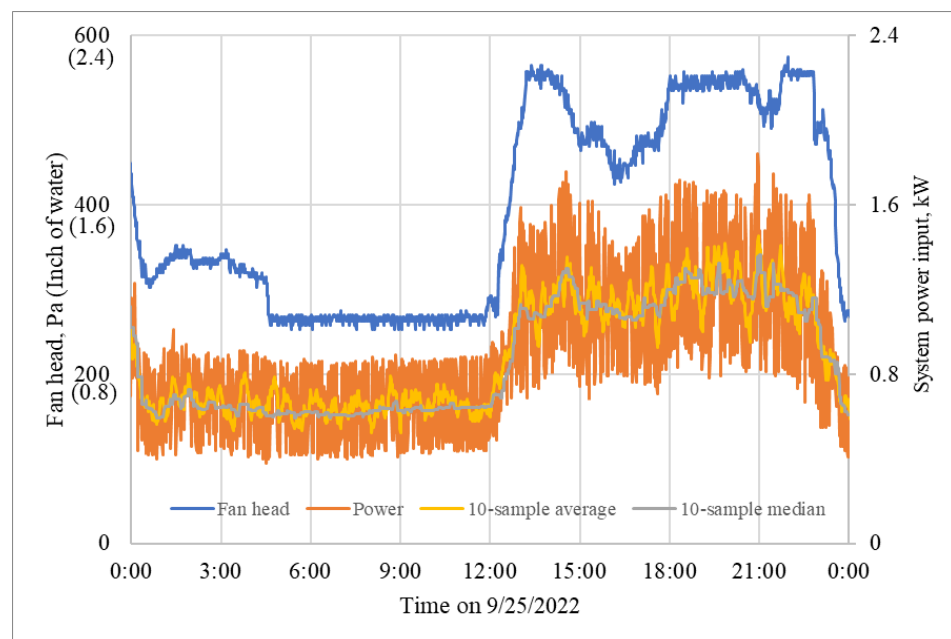
The measured system performance data is presented as the fan head–airflow correlation and the system power input–airflow correlation at various fan speeds. Figure 8a shows the measured fan head versus airflow rate, while Figure 8b shows the measured median system power input versus airflow rate in eight different fan speed ranges, i.e., 71–72%, 74–76%, 79–81%, 84–86%, 89–91%, 94–96%, 98–99%, and 100%, differentiated by different colors.

According to the affinity laws, defined by Equations (5a)–(5c), the fan head–air flow and the fan power curve–airflow curves at an actual speed is converted from these curves at the full design speed based on the fan speed using Equations (6) and (7), as shown in Figure 3a. Thus, the fan speed directly impacts the fan head curve and shaft power curve. On the other hand, the drive efficiency, which is the ratio of the fan shaft power to the system power input, is related to the fan speed, defined by Equation (12). Thus, the fan speed impacts the drive efficiency and, consequently, indirectly impacts the system power input through the fan speed-related drive efficiency. Figure 8 clearly reveals the direct

impacts of the fan speed on the fan head (a) and both the direct and indirect impacts of the fan speed on the system power input (b).



(a) Fan airflow rate and speed



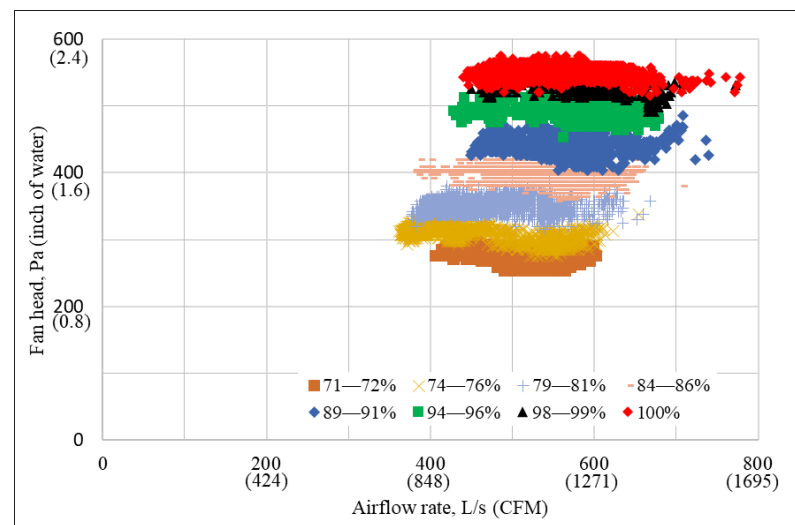
(b) Fan head and system power input

**Figure 7.** Measured fan performance data versus time.

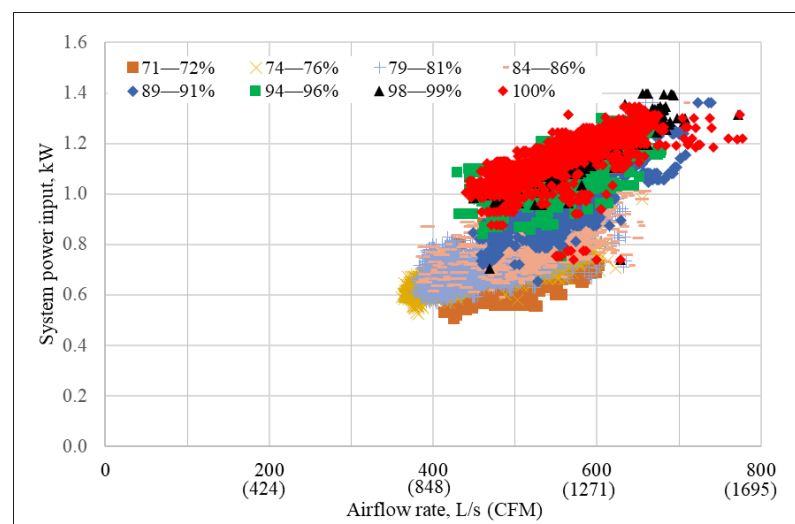
### 3.3. Data Analysis

#### 3.3.1. Manipulated Performance Data at the Full Design Speed

To intentionally eliminate the direct impacts of the variable fan speed, the affinity laws, defined by Equations (5a)–(5c), were applied to convert the raw fan performance data at all fan speeds to the fan performance data at the full design speed. Figure 9a shows the converted fan head versus airflow rate data and Figure 9b shows the converted system power input versus airflow rate data at the full design speed.



(a) Fan head versus fan airflow



(b) System power input versus fan airflow

**Figure 8.** Fan head and system power input versus airflow at various fan speed ranges.

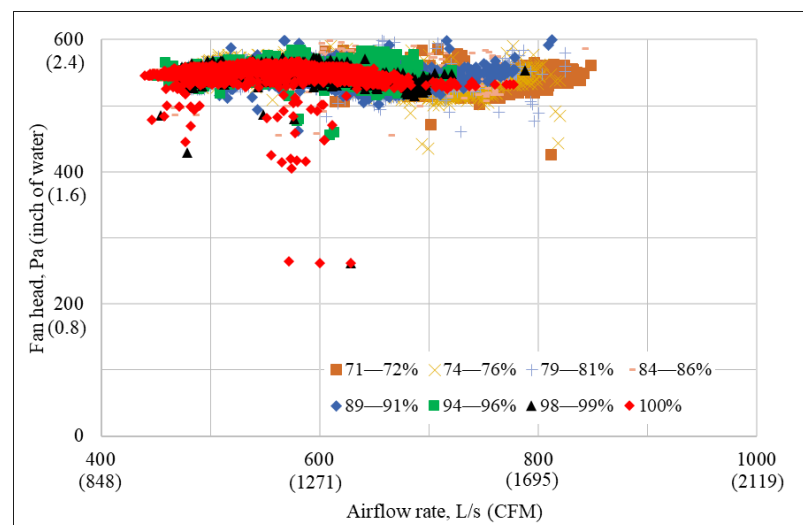
As a result, the converted fan head versus fan airflow rate data at the full design speed in Figure 9a becomes more consistent. The wide band is the result of chaotic changes in pressure and flow velocity in the turbulent flow pattern. On the other hand, the converted system power input versus fan airflow rate data at the full design speed in Figure 9b is still slightly impacted by the fan speed indirectly through the fan speed-related drive efficiency. In addition to the turbulent flow impact, the system dynamic operation also contributes to the wide band. The 10-sample median of the one-minute power samples cannot perfectly catch the system dynamic operation, reflected by the slight mismatch between the fan speed and power in Figure 7. As recommended previously, the system power input with a shorter sampling time can eliminate the mismatch.

The fan head-airflow curve at the full design speed converted from the data at all the fan speeds is shown in Figure 10. The first step in the identification approach can be done by regressing this fan head curve in Figure 10:

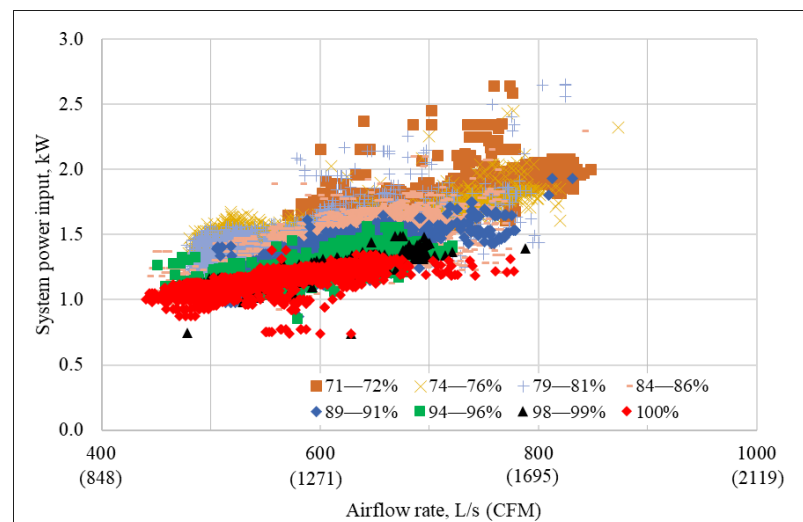
$$H_d = -0.0519 \cdot Q_d + 578.42 \quad (20)$$

where the fan airflow is in L/s and the fan head is in Pa.





(a) Fan head versus airflow rate



(b) System power input versus fan airflow rate

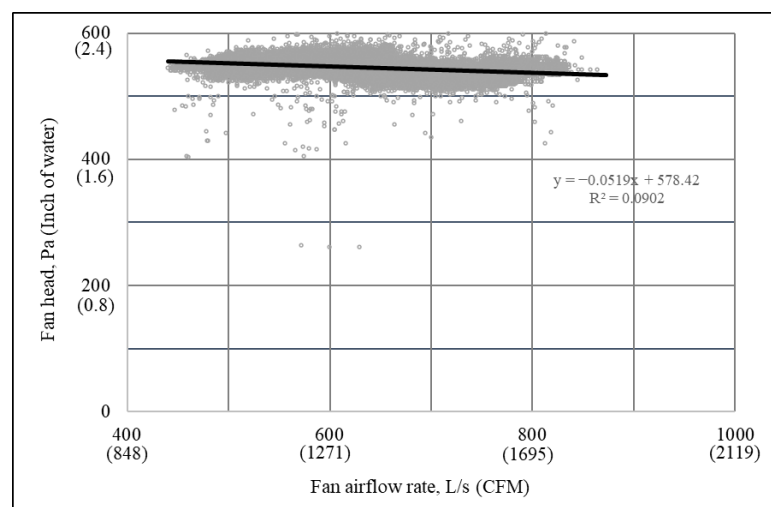
**Figure 9.** Fan head and system power input versus airflow rate at the full design speed.**Figure 10.** Fan head curve at the full design speed.

Figure 9a also shows that the fan head curve converted from the data at lower fan speeds locates on the right and the fan head curve converted from the data at higher fan speeds locates on the left. This is the reason to use the operation data at all speeds with affinity laws to create the fan head curve. Moreover, it is noted that the regressed linear fan head curve is an actual operational curve limited by system design and operation condition, which is only a part of the entire fan head curve.

On the other hand, the converted system power input versus fan airflow rate data at the full design speed in Figure 9b is differentiated by the fan speed. Before the fan shaft power curve can be identified, the drive efficiency needs to be identified and applied to further convert the system power input to the fan shaft power by eliminating the indirect impact of the fan speed through the drive efficiency.

### 3.3.2. Speed-Independent Fan-Efficiency Curve

First, to obtain the fan speed-independent equivalent fan efficiency, the system efficiency was calculated based on Equation (13) and is presented versus the ratio of the fan head to fan airflow rate squared in Figure 11. The increased system efficiency at higher fan speeds means that the drive efficiency increases as the fan speed increases.

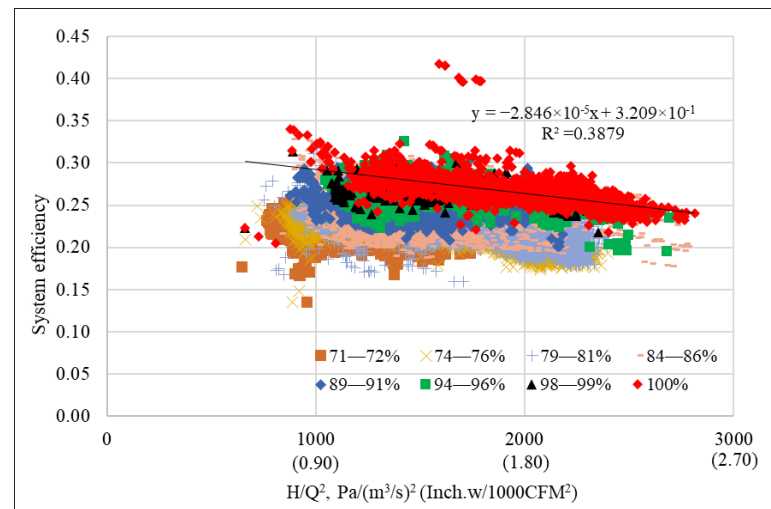


Figure 11. System efficiency versus the ratio of fan head to fan airflow squared.

Second, the system efficiency (red markers) at the full design speed represent the equivalent fan efficiency according to Equation (14). The second step in the identification approach can be done by regressing the equivalent fan-efficiency curve as a function of the ratio of the fan head to fan airflow squared:

$$\eta_{fan,e} = \eta_{sys@w=1} = -2.846 \times 10^{-5} \cdot \left( \frac{H}{Q^2} \right) + 0.3209 \quad (21)$$

where the fan airflow rate ( $Q$ ) is in L/s and the fan head ( $H$ ) is in Pa.

Like the fan head curve at the full design speed, the equivalent fan-efficiency curve is regressed as a linear curve limited by system design and operation condition, which is only a part of the entire equivalent fan-efficiency curve.

It is important to highlight that the fan efficiency in Equation (21) is independent of the fan speed and Equation (21) can be applied to calculate the fan efficiency at any fan speed even though it is obtained from the test data at the full design speed.

### 3.3.3. Drive-Efficiency Curve

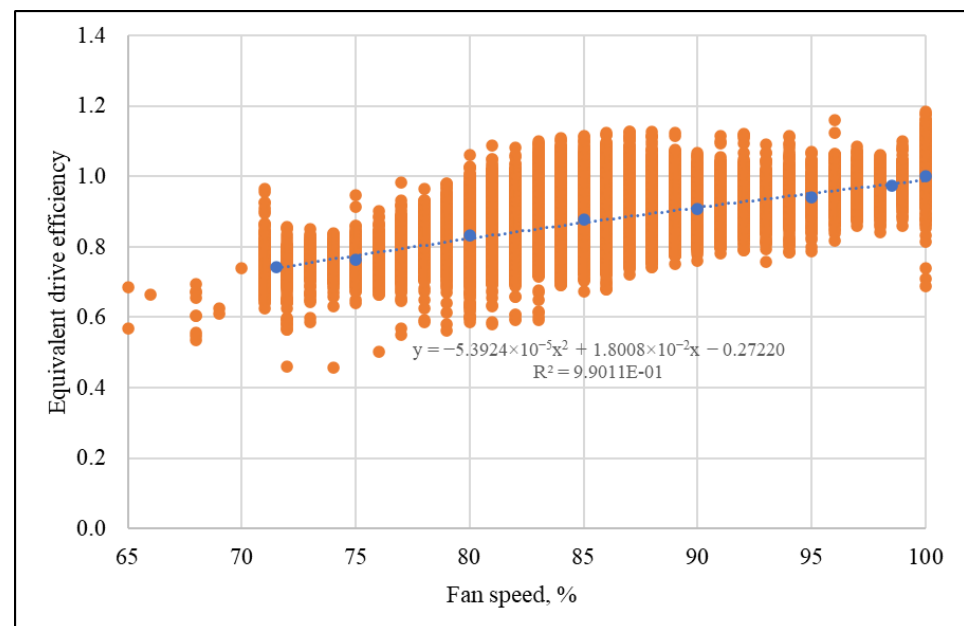
Since the system efficiency is the product of the equivalent fan efficiency and the equivalent drive efficiency, the equivalent drive efficiency can be readily calculated using

Equation (16), in which the system efficiency is shown in Figure 11 and the equivalent fan efficiency is defined by Equation (21).

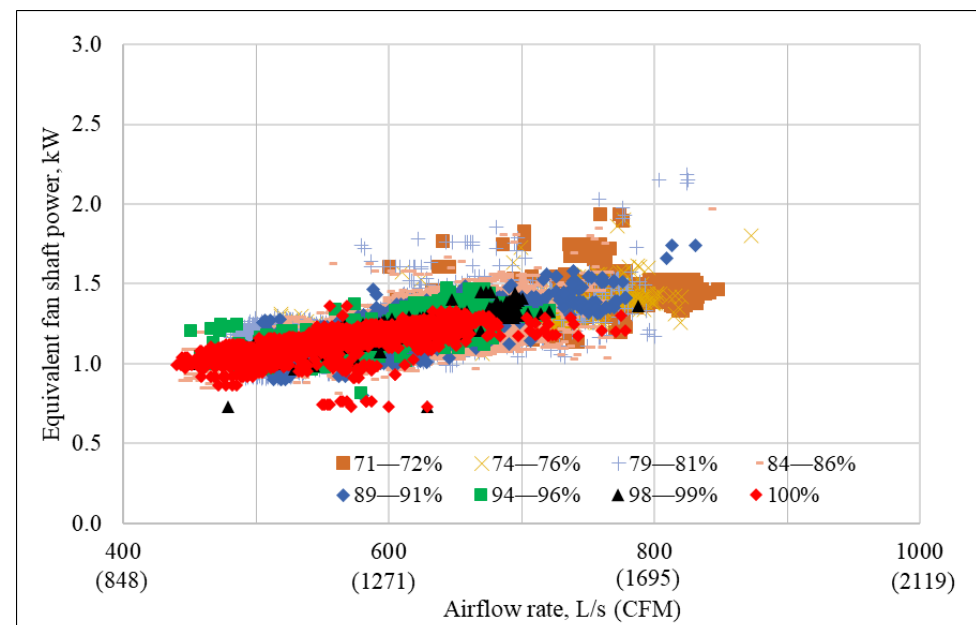
Figure 12a shows the equivalent drive efficiency (orange markers) calculated using the data at all fan speeds and the average equivalent drive efficiencies calculated using the data at eight fan speed ranges in Figures 8, 9 and 11. Thus, the third step in the identification approach can be done by regressing the average equivalent drive-efficiency curve as a function of the fan speed.

$$\eta_{drive,e} = -5.3924 \times 10^{-5} \omega^2 + 1.8008 \times 10^{-2} \omega - 0.27220 \quad (22)$$

where the fan speed ( $\omega$ ) is in percentage.



(a) Equivalent drive efficiency versus fan speed



(b) Equivalent fan shaft power curve at the full design speed

**Figure 12.** Equivalent drive efficiency and equivalent fan shaft power curve.

It should be noted that not only the system dynamics but also the oscillations of the VFD PWM output power result in the wide band of the equivalent drive-efficiency curve in Figure 12a.

### 3.3.4. Fan Shaft Power Curve

With the regressed equivalent drive efficiency, defined by Equation (22), the system power input in Figure 9b can be converted to the equivalent fan shaft power using Equation (19). Figure 12b shows the equivalent fan shaft power versus airflow rate curve at the full design speed. Like the converted fan head versus fan airflow rate data at the full design speed in Figure 9a, the converted equivalent fan shaft power versus airflow rate data in Figure 12b becomes more consistent after eliminating the indirect impact of the variable fan speed through the fan speed-related drive efficiency.

The equivalent fan shaft power versus airflow rate curve at the full design speed converted from the data at all the fan speeds is shown in Figure 13 and can be regressed as:

$$W_{sh,e} = 0.0012 \cdot Q + 0.482 \quad (23)$$

where the fan airflow rate is in L/s and the equivalent fan shaft power is in kW. The fourth step in the identification approach is completed.

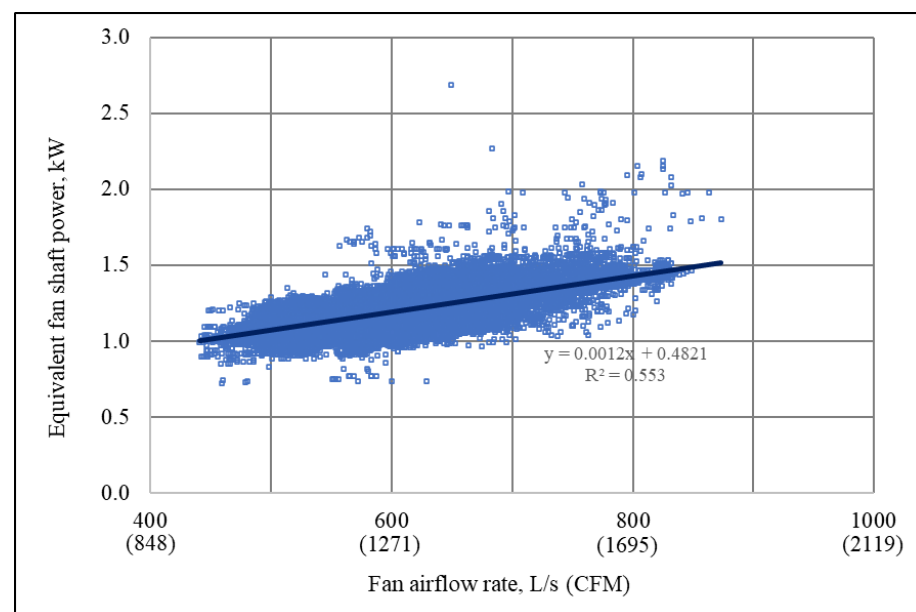
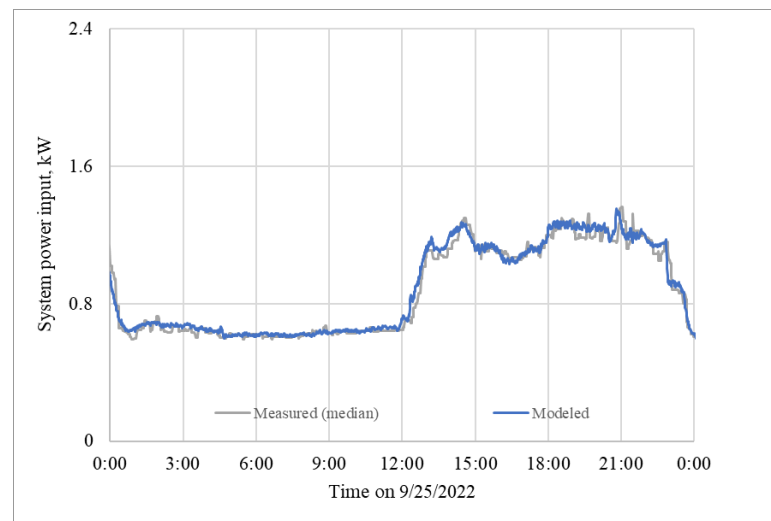


**Figure 13.** Equivalent shaft power curves at the full design speed.

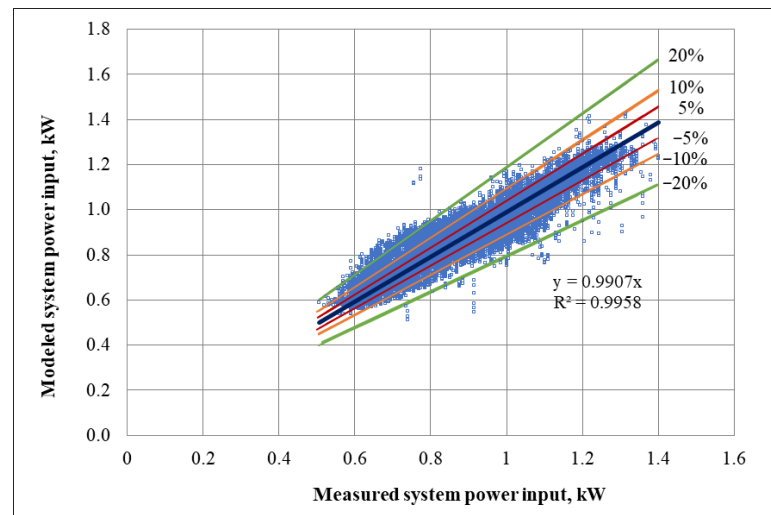
### 3.3.5. Energy Model and Overall Error Evaluation

Overall, the fan head curve shown in Figure 10 and defined by Equation (20), the equivalent fan-efficiency curve shown in Figure 11a and defined by Equation (21), and the equivalent drive-efficiency curve shown in Figure 12a and defined by Equation (22) configure the energy model of the studied VFD–motor–fan system. The equivalent fan shaft power curve shown in Figure 13 and defined by Equation (23) is dependent on the fan head curve and the equivalent fan-efficiency curve. The system efficiency can be obtained from the equivalent drive-efficiency curve and equivalent fan-efficiency curve and is applied to model the system power input based on the fan airflow and head using Equation (17).

The overall error of the identified energy model can be evaluated by comparing the modeled system power input and the measured system power input. Figure 14a shows the comparison over a one-day period and Figure 14b shows the modeled system input versus measured system power input with 5%, 10% and 20% discrepancies over the entire identification period. The root mean squared error is 55 W or 4% with respect to the maximum median system power input, 1.3 kW.



(a) Comparison versus time



(b) Modeled power versus measured power

**Figure 14.** Comparison of modeled and measured system power input.

#### 4. Applications

The identified energy model of the studied system is applied to detect the slipped belt faults and to develop a virtual fan airflow meter with the measurements of the fan head, speed, and system power input. To demonstrate general applications, the fan airflow rate was not treated as an input in these applications since most AHUs do not have a permanently installed airflow meter even though the test AHU has one. The system performance data from 1 August to 13 September 2022 are applied to demonstrate the slipped belt fault detection, while the system performance data from 26 October to 31 October 2022 are applied to demonstrate the virtual fan flow meter development; besides these two applications, the developed energy model can potentially be applied for the system power input simulation, as calculated system power input based on the fan airflow and head, shown in Figure 14.

##### 4.1. Fault Detection

The fault-free fan head versus equivalent shaft power curve at the full design speed ( $\omega = 1$ ), associated with Equation (8), can be obtained from the identified fan head and equivalent shaft power curves, defined by Equations (20) and (23), and is shown by orange



circles in Figure 15. The fault-free fan head versus equivalent shaft power curve at the full design speed can be regressed as:

$$H_d = -43.833W_{sh,e} + 598.97 \quad (24)$$

where the equivalent fan shaft power is in kW and the fan head is in Pa.

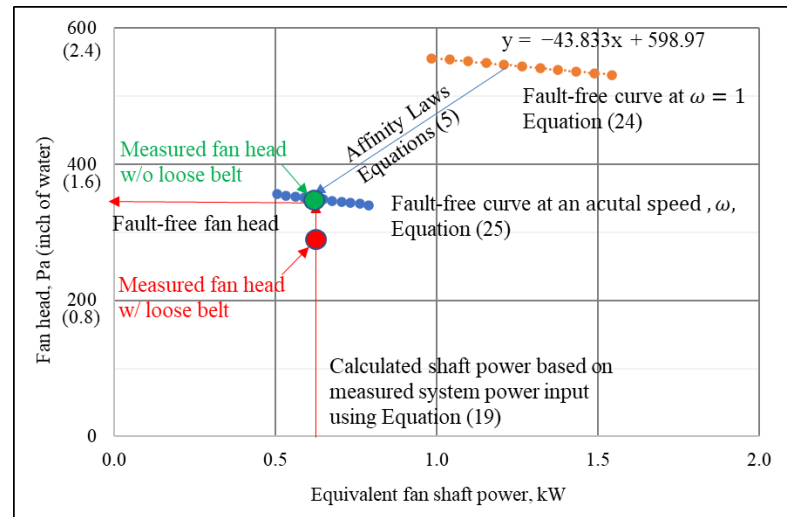


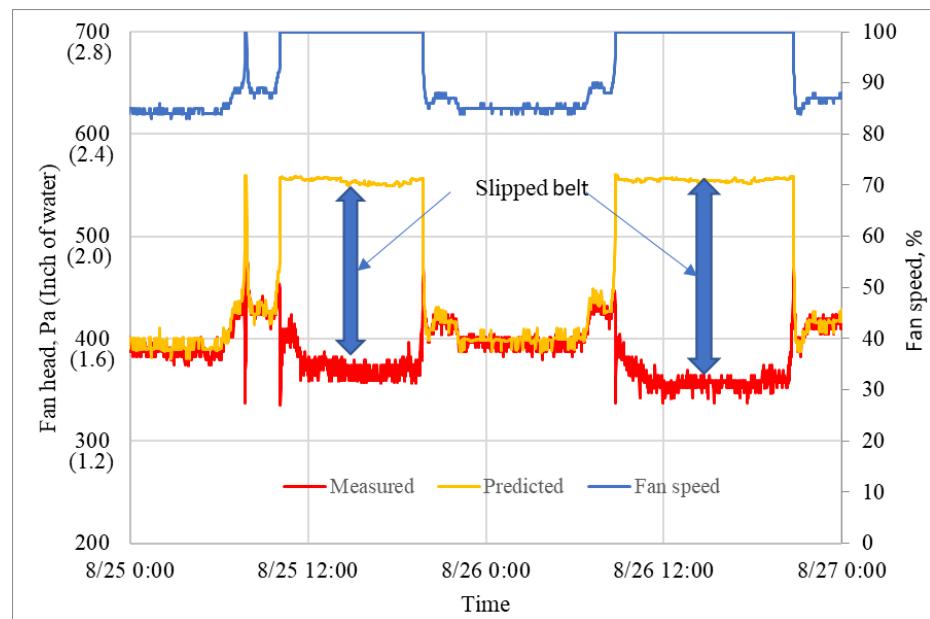
**Figure 15.** Fan head versus equivalent shaft power curve at the full design speed.

A two-step slipped belt fault-detection approach is developed for each operation point defined by the fan head, speed, and system power input, as shown in Figure 15. In Step one, the fault-free fan head in Equation (25) can be predicted based on available fan speed and system power input. First the equivalent shaft power is calculated based on measured system power input using Equation (19) by applying the equivalent drive-efficiency curve, defined by Equation (22). Then the fault-free fan head-shaft power curve at any speed, shown by blue circles in Figure 15, can be converted from the curve at the full design speed, defined by Equation (24), by applying the affinity laws, defined by Equations (5a)–(5c).

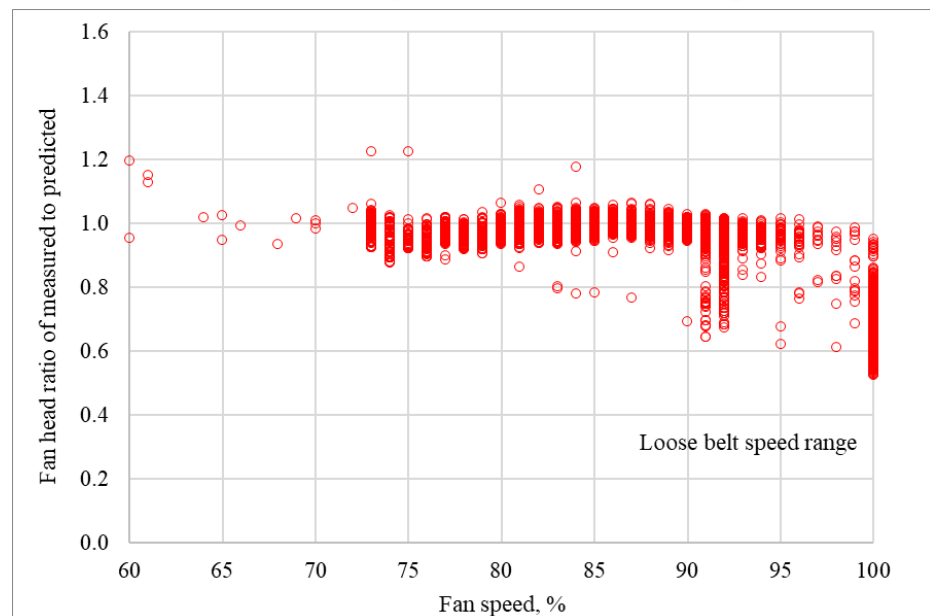
$$H = \left( -43.833 \cdot \frac{W_{sys} \cdot \eta_{drive,e}(\omega)}{\omega^3} + 598.97 \right) \cdot \omega^2 \quad (25)$$

In Step 2, the fault-free fan head is compared with the measured fan head. The belt operates normally if the measured fan head is close to the predicted fault-free fan head, as shown by the green point in Figure 15. On the other hand, when the belt is loose, the fan cannot provide enough head and consequently the measured fan head is much lower than the predicted fault-free fan head, as shown by the red point in Figure 15. Thus, the ratio of the measured fan head to the predicted fault-free fan head indicates the operation status of the belt. The fault-free ratio should be close to unity. On the other hand, the slipped belt will result in the ratio less than a threshold, such as 80%.

The developed slipped belt fault-detection algorithm is applied to the performance data. Figure 16a compares the predicted (yellow) and measured (red) fan head along with the fan speed (blue) in a two-day period and Figure 16b shows the ratio of the measured predicted fan head to the predicted measured fan head versus the fan speed in the entire test period. The deviation of the predicted fault-free fan head from the measured fan head in Figure 16a and the deviation of the fan head ratio from unity in Figure 16b indicates the slipped belt. Moreover, Figure 16b also reveals that the slipped belt status only occurred at the high fan speed from 90% to 100% full design speed even though the belt was slipped, which matches with the investigation conducted by Wang et al. [29]. This means that the slipped belt detection needs to be conducted at higher fan speeds.



(a) Fan head comparison along with fan speed



(b) Ratio versus fan speed in the entire test period

**Figure 16.** Slipped belt fault detection.

The proposed loose belt fault-detection approach utilizes the simple mathematical expression, defined by Equation (25), and can be readily implemented in the BAS. Of course, the simple physical equation needs to be calibrated through experiments.

#### 4.2. Virtual Flow Meter Development

The airflow rate is required at AHUs for optimal operation on duct static pressure control, building pressure control, outdoor air control, and cooling demand control. However, in general, the airflow meter is not a conventional meter installed at AHUs. With the identified energy model defined by the fan head and equivalent fan efficiency shaft power curves along with the equivalent drive-efficiency curve, a virtual fan flow meter can be developed to calculate the fan airflow rate based on the measured fan head, speed, and system power input. A three-step approach is followed:

1. The equivalent drive efficiency is determined by the available fan speed using Equation (22) and is applied to calculate the equivalent fan shaft power using Equation (19);
2. According to the affinity laws, the equivalent fan efficiency can be represented as a function of the ratio of the equivalent shaft power to the fan head to the power of 1.5, as shown by Equation (11), independent of the fan airflow rate. Based on the identified fan head and equivalent shaft power curves shown in Figures 10 and 13, the equivalent fan efficiency is presented by orange circles in Figure 17 and is regressed as:

$$\eta_{fan,e} = -0.017 \cdot \left( \frac{W_{sh,e}}{H^{1.5}} \right)^2 + 0.1501 \cdot \left( \frac{W_{sh,e}}{H^{1.5}} \right) - 0.0192 \quad (26)$$

where the equivalent fan shaft power is in kW and the fan head is in kPa.

3. The fan airflow rate can be calculated virtually from the measured fan head, speed, and system power input.

$$Q = \frac{W_{sys} \cdot \eta_{drive,e}(\omega) \cdot \eta_{fan,e}(W_{sys} \cdot \eta_{drive,e} / H^{1.5})}{H} \quad (27)$$

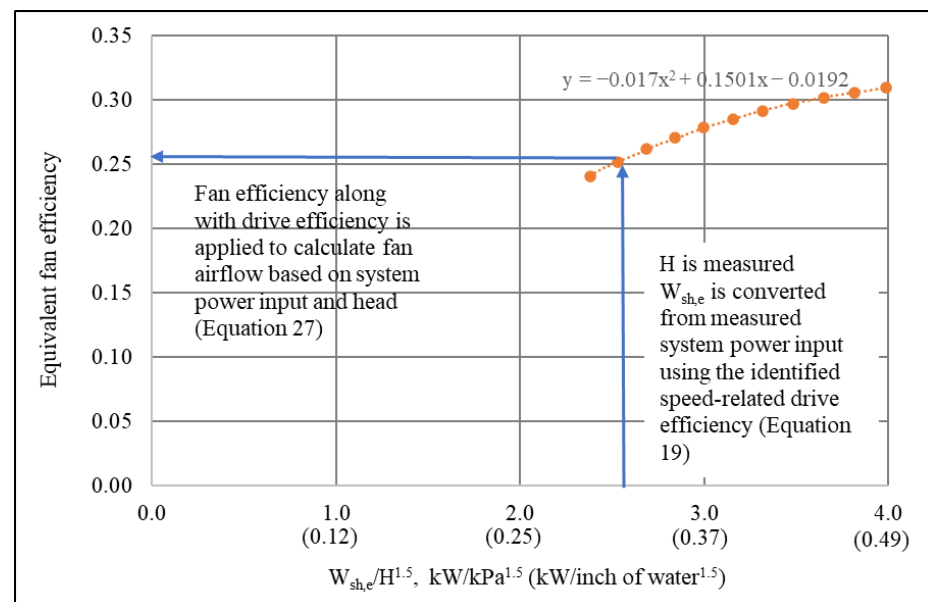


**Figure 17.** Fan efficiency versus the ratio of fan shaft power to fan head to the power of 1.5.

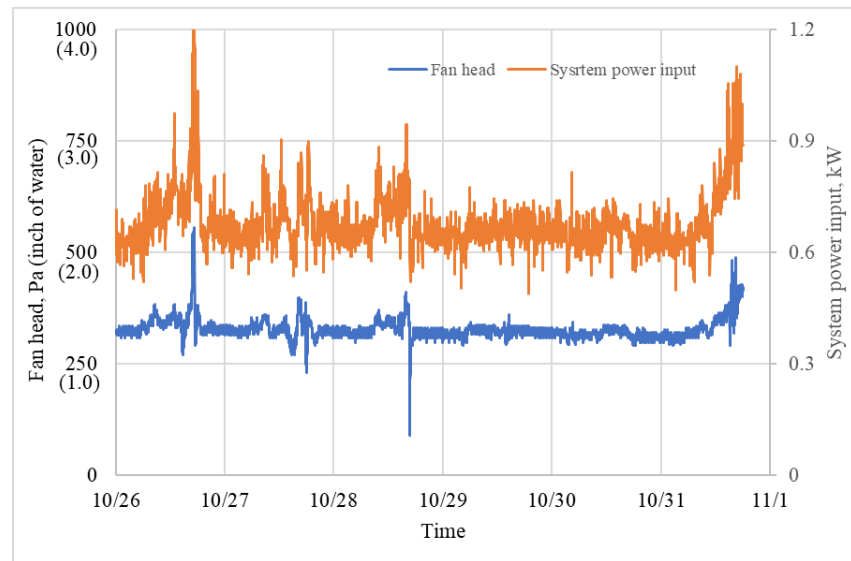
Figure 18a shows the measured fan head (blue) and system power input (orange) and Figure 18b shows the measured fan speed (orange) as well as the calculated equivalent drive efficiency (blue) using Equation (22) and the calculated equivalent fan efficiency (gray) using Equation (26) in the virtual fan flow meter demonstration period.

Figure 19 compares the fan airflow rates measured by the physical airflow meter (blue) and calculated by the developed virtual airflow meter (orange) using Equation (27). The root mean squared error is 42 L/s (90 CFM) or 4% with respect to the design fan airflow rate, 1200 L/s (2500 CFM), which results in a major way from the oscillations of the VFD PWM output power.

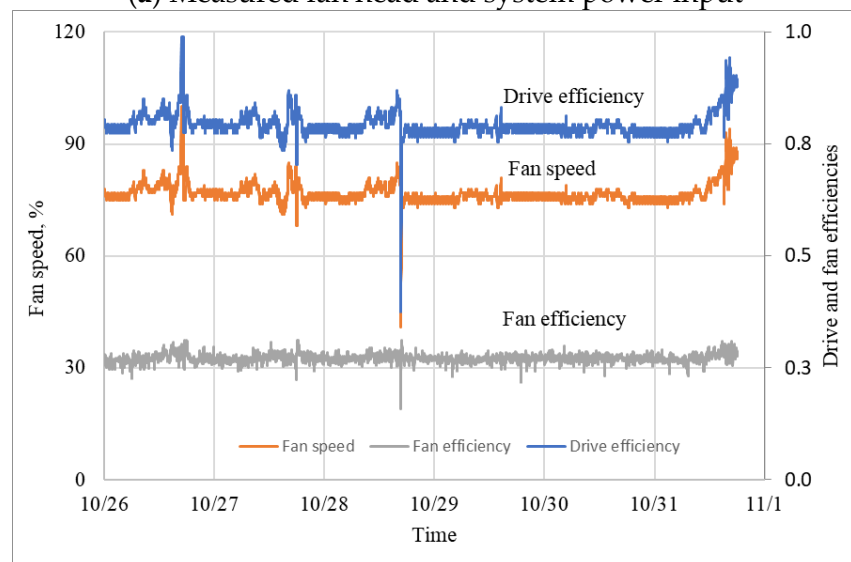
#### 4.3. Discussion on Alternative Power Measurement

The VFD for large-sized motors can provide consistent VFD output power, which has a stable value by the filter inside the VFD. Figure 20 compares the motor power input read from a VFD and the motor power input measured by a power analyzer for a 5.6 kW (7.5 HP) motor [39]. It reveals that the VFD output power measured by the VFD is different from the actual VFD output power but has a consistent correlation with actual VFD output

power. Thus, the VFD output power read from the VFD can still be applied to detect faults and develop virtual flow meters through a calibration process.



(a) Measured fan head and system power input



(b) Measured fan speed and calculated equivalent drive and fan efficiencies

**Figure 18.** Inputs and efficiencies for the virtual flow meter.

In this case, a conventional power meter is not required and the VFD output power, which is also the motor input power ( $W_{\text{motor}}$ ), as shown in Figure 1, can replace the system power input ( $W_{\text{sys}}$ ). The developed identification and application approaches can be applied in this case except that the drive efficiency ( $\eta_{\text{drive}}$ ), defined by Equation (12), must be replaced by the motor-belt efficiency ( $\eta_{\text{mb}}$ ), which is the product of the motor efficiency and belt efficiency.

$$\eta_{\text{mb}} = \frac{W_{\text{sh}}}{W_{\text{motor}}} = f_{\text{mb}}(\omega) \quad (28)$$

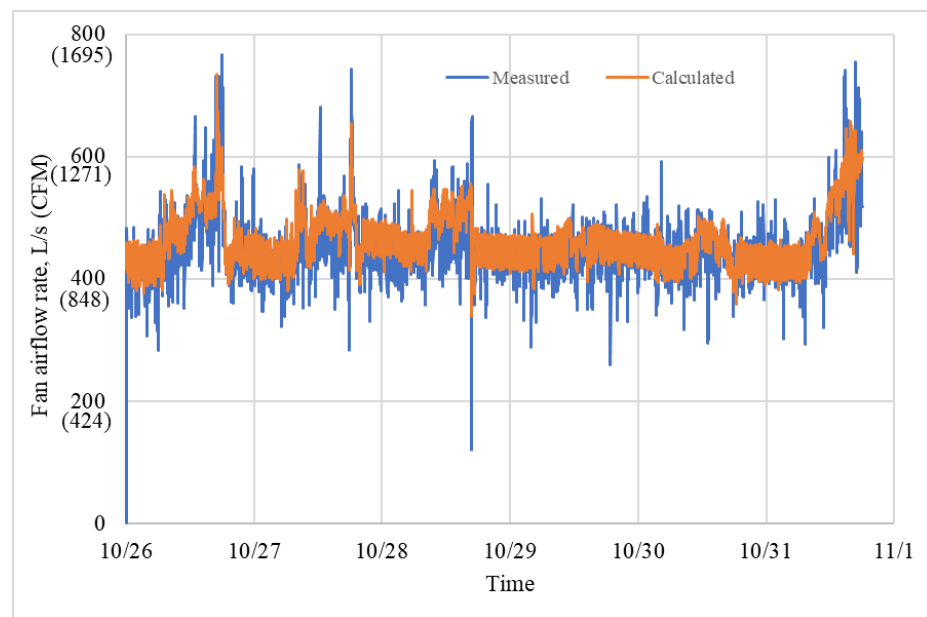


Figure 19. Validation of the virtual flow meter.

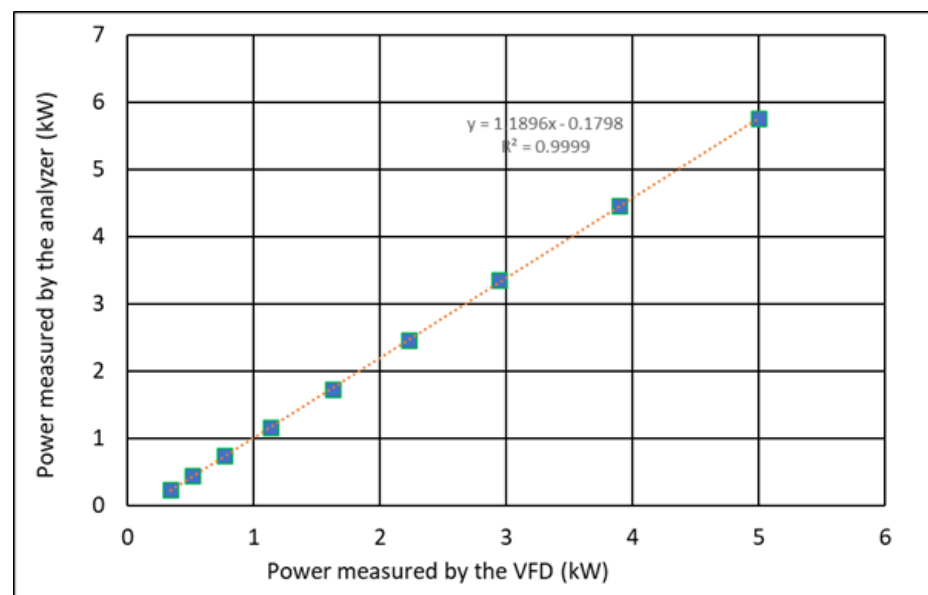


Figure 20. Comparison of VFD power reading and measured motor power input.

## 5. Conclusions

In this paper, a four-step identification approach was developed to obtain the energy model of an existing VFD–motor–fan system without measuring the fan shaft power. The developed approach provides a method to obtain the accurate drive-efficiency function, which covers the impact of VFDs on motor efficiency, based on the actual operation data and, consequently, generate the accurate energy model for VFD–motor–fan systems. This data-drive energy model advances EnergyPlus, which provides the drive efficiency with an error of 10–25% by ignoring the impact of VFDs on motor efficiency. With the developed approach, the fan head-airflow rate curve and the equivalent fan shaft power-airflow rate curve at the full design speed, the two speed-independent equivalent fan-efficiency curves and the equivalent drive efficiency–fan speed curve were identified for an existing VFD–motor–fan system with the design fan airflow rate of 1200 L/s (2500 CFM) based on the measured fan head, speed, and system power input as well as temporarily measured



airflow rate. The root mean squared error of the energy model is 55 W or 4% with respect to the maximum system power input, 1.3 kW.

Three techniques play a key role to identify the fan efficiency and drive system curves without the fan shaft power measurement. The first one is to use the system efficiency, which can always be calculated based on available fan head, speed, and system power input, to avoid the fan shaft power measurement. The second one is to introduce the equivalent fan efficiency and equivalent drive efficiency. The unknown constant drive efficiency at the full design speed is merged into both the equivalent efficiencies. The third one is to express the equivalent fan efficiency as a function of the ratio of the fan head to the fan airflow squared using the affinity laws and the equivalent drive efficiency as a function of the fan speed by consolidating three influencing factors (i.e., the fan shaft power, VFD output voltage, and frequency). Two efficiency functions are uncorrelated.

The identified accurate energy model was then applied to detect the slipped belt faults by a two-step fault-detection approach and to develop a virtual fan flow meter by a three-step approach using the measured fan speed, head, and system power input using simple mathematic expressions which can be readily implemented in building automation systems. The developed fault-detection algorithm can effectively detect the slipped belt faults by comparing the fault-free fan head with the measured fan head and the developed virtual flow meter can accurately calculate the fan supply airflow rate based on the measured fan speed and head and system power input with the root mean squared error of 42 L/s (90 CFM) in the studied system.

**Author Contributions:** Writing—original draft preparation, investigation and supervision, G.W.; data collection, discussion, writing—reviewing and editing, N.T.; data collection, discussion, writing—reviewing and editing, J.W.; discussion, writing—reviewing and editing, Z.W.; writing—reviewing, editing and supervision, L.S. All authors have read and agreed to the published version of the manuscript.

**Funding:** This research was funded by the U.S. Department of Energy’s Office of Energy Efficiency and Renewable Energy (EERE) under the Building Technologies Office (award number DE-EE0008683). The views expressed herein do not necessarily represent the views of the U.S. Department of Energy or the United States Government.

**Institutional Review Board Statement:** Not applicable.

**Informed Consent Statement:** Not applicable.

**Data Availability Statement:** Data will be made available on request.

**Conflicts of Interest:** The authors declare no conflict of interest.

## Nomenclature

$f$	=general function or VFD output frequency
$H$	=fan head, Pa, kPa, or inch of water
$Q$	=fan airflow rate, L/s, m <sup>3</sup> /s, or CFM
$W$	=power, kW
$\omega$	=relative fan speed
$\eta$	=efficiency

### Subscripts:

d	=full design speed
e	=equivalent
mb	=motor-belt
sh	=shaft
sys	=drive system

## References

- DOE. *Energy Savings Potential and Opportunities for High-Efficiency Electric Motors in Residential and Commercial Equipment*; The U.S. Department of Energy Building Technologies Office: Washington, DC, USA, 2013.
- Friedman, H.; Shuman, M.; Claridge, D.; Curtain, J.; Hayes, P. *Building Commissioning: Innovation to Practice Technical Report*; PIER Energy-Related Environmental Research Program; CEC-500-2008-074; California Energy Commission: Sacramento, CA, USA, 2007.
- Dong, J.; Im, P.; Huang, S.; Chen, Y.; Munk, J.D.; Kuruganti, T. *Development and Calibration of an Online Energy Model for AHU Fan*; Oak Ridge National Lab. (ORNL): Oak Ridge, TN, USA, 2019.
- Hughes, A. *Electric Motors and Drives: Fundamentals, Types and Applications*, 2nd ed.; Newnes: Burlington, MA, USA, 2006.
- McQuiston, F.C.; Parker, J.D.; Spitler, J.D. *Heating, Ventilating, and Air Conditioning: Analysis and Design*; John Wiley & Sons: Hoboken, NJ, USA, 2004.
- DOE. *A Sourcebook for Industry: Improving Motor and Drive System Performance*; The U.S. Department of Energy (DOE) Office of Energy Efficiency and Renewable Energy: Washington, DC, USA, 2008.
- Qiu, W.; Ouyang, Z. Energy Efficient Control of Parallel Variable-Frequency Pumps in Magnetic Water-Cooling System. *J. Fluids Eng.* **2019**, *142*, 024502. [\[CrossRef\]](#)
- Mallios, Z.; Siarkos, I.; Karagiannopoulos, P.; Tsiarapas, A. Pumping energy consumption minimization through simulation-optimization modelling. *J. Hydrol.* **2022**, *612*, 128062. [\[CrossRef\]](#)
- Kong, L.; Li, Y.; Tang, H.; Yuan, S.; Yang, Q.; Ji, Q.; Li, Z.; Chen, R. Predictive control for the operation of cascade pumping stations in water supply canal systems considering energy consumption and costs. *Appl. Energy* **2023**, *341*, 121103. [\[CrossRef\]](#)
- Wijaya, T.K.; Alhamid, M.I.; Saito, K.; Nasruddin, N. Dynamic optimization of chilled water pump operation to reduce HVAC energy consumption. *Therm. Sci. Eng. Prog.* **2022**, *36*, 101512. [\[CrossRef\]](#)
- Afram, A.; Janabi-Sharifi, F. Review of modeling methods for HVAC systems. *Appl. Therm. Eng.* **2014**, *67*, 507–519. [\[CrossRef\]](#)
- Ji, L.; Li, W.; Shi, W.; Tian, F.; Agarwal, R. Diagnosis of internal energy characteristics of mixed-flow pump within stall region based on entropy production analysis model. *Int. Commun. Heat Mass Transf.* **2020**, *117*, 104784. [\[CrossRef\]](#)
- Shankar, V.K.A.; Subramaniam, U.; Elavarasan, R.M.; Raju, K.; Shanmugam, P. Sensorless parameter estimation of VFD based cascade centrifugal pumping system using automatic pump curve adaption method. *Energy Rep.* **2021**, *7*, 453–466. [\[CrossRef\]](#)
- Pan, Y.; Huang, Z.; Wu, G. Calibrated building energy simulation and its application in a high-rise commercial building in Shanghai. *Energy Build.* **2007**, *39*, 651–657. [\[CrossRef\]](#)
- Chilundo, R.J.; Maure, G.A.; Mahanjane, U.S. Dynamic mathematical model design of photovoltaic water pumping systems for horticultural crops irrigation: A guide to electrical energy potential assessment for increase access to electrical energy. *J. Clean. Prod.* **2019**, *238*, 117878. [\[CrossRef\]](#)
- Saidur, R.; Mekhilef, S. Energy use, energy savings and emission analysis in the Malaysian rubber producing industries. *Appl. Energy* **2010**, *87*, 2746–2758. [\[CrossRef\]](#)
- Saidur, R.; Mekhilef, S.; Ali, M.B.; Safari, A.; Mohammed, H.A. Applications of variable speed drive (VSD) in electrical motors energy savings. *Renew. Sustain. Energy Rev.* **2012**, *16*, 543–550. [\[CrossRef\]](#)
- Viholainen, J.; Tamminen, J.; Ahonen, T.; Ahola, J.; Vakkilainen, E.; Soukka, R. Energy-efficient control strategy for variable speed-driven parallel pumping systems. *Energy Effic.* **2013**, *6*, 495–509. [\[CrossRef\]](#)
- Wang, X.; Zhao, Q.; Wang, Y. An asynchronous distributed optimization method for energy saving of parallel-connected pumps in HVAC systems. *Results Control. Optim.* **2020**, *1*, 100001. [\[CrossRef\]](#)
- IEEE Standard Test Procedure for Polyphase Induction Motors and Generators. *IEEE Std 112™-2017*; Institute of Electrical and Electronics Engineers: New York, NY, USA, 2017.
- Stein, J.; Hydeman, M.M. Development and Testing of the Characteristic Curve Fan Model. *ASHRAE Trans.* **2004**, *110*, 347.
- DOE. *EnergyPlus™ Version 8.5 Documentation: Engineering Reference*; U.S. Department of Energy: Washington, DC, USA, 2016.
- DOE. *The Fan System Assessment Tool (FSAT)*; Industrial Technologies Program (ITP); U.S. Department of Energy: Washington, DC, USA, 2010.
- DOE. *The Pumping System Assessment Tool (PSAT)*; Industrial Technologies Program (ITP); U.S. Department of Energy: Washington, DC, USA, 2010.
- Wildi, T. *Electrical Machines, Drives and Power Systems*; Pearson Education, Inc.: Upper Saddle River, NJ, USA, 2002.
- Domijan, A.; Abu-aisheh, A.; Czarkowski, D. Efficiency and separation of losses of an induction motor and its adjustable-speed drive at different loading/speed combinations. *ASHRAE Trans.* **1997**, *103*, 228–234.
- Gao, X.; McNerny, S.A.; Kavanaugh, S.P. Efficiencies of an 11.2 kW variable speed motor and drive. *ASHRAE Trans.* **2001**, *107*, 259.
- Burt, C.M.; Piao, X.; Gaudi, F.; Busch, B.; Taufik, N.F. Electric motor efficiency under variable frequencies and loads. *J. Irrig. Drain. Eng.* **2008**, *134*, 129–136. [\[CrossRef\]](#)
- Wang, F.; Yoshida, H.; Miyata, M. Total Energy Consumption Model of Fan Subsystem Suitable for Continuous Commissioning. *ASHRAE Trans.* **2004**, *110*, 357.
- Ding, L.; Ding, L.; Wang, G. Experimental Investigation of Induction Motor Power Factor and Efficiency Impacted by Pulse Width Modulation Power and Voltage Controls of Variable-Frequency Drives. *ASHRAE Trans.* **2021**, *127*, 817–828.

31. DOE. *Energy Tips: Motor Systems (Tip Sheet #11)*; The U.S. Department of Energy Advanced Manufacturing Office of Energy Efficiency and Renewable Energy: Washington, DC, USA, 2012.
32. Krukowski, A.; Wray, C.P. Standardizing data for VFD. *ASHRAE J.* **2013**, *55*, 8–10.
33. Mei, L.; Levermore, G. Simulation and validation of a VAV system with an ANN fan model and a non-linear VAV box model. *Build. Environ.* **2002**, *37*, 277–284. [[CrossRef](#)]
34. Brambley, M.R.; Fernandez, N.; Wang, W.; Cort, K.A.; Cho, H.; Ngo, H.; Goddard, J.K. *Final Project Report: Self-Correcting Controls for Vav System Faults Filter/Fan/Coil and Vav Box Sections*; Pacific Northwest National Lab. (PNNL): Richland, WA, USA, 2011.
35. Tukur, A.; Hallinan, K.P. Statistically informed static pressure control in multiple-zone VAV systems. *Energy Build.* **2017**, *135*, 244–252. [[CrossRef](#)]
36. Pang, X.; Liu, M.; Zheng, B. Building pressure control in VAV system with relief air fan. In Proceedings of the Fifth International Conference for Enhanced Building Operations, Pittsburgh, PA, USA, 11–13 October 2005.
37. Phalak, K.; Wang, G. Minimum outdoor air control and building pressurization with lack of airflow and pressure sensors in air-handling units. *J. Archit. Eng.* **2016**, *22*, 04015017. [[CrossRef](#)]
38. Hurt, R.; Wang, Z.; Wang, G.; Andiroglu, E.; Song, L. Preliminary Investigation of Active Demand Flexibility Control at Air-Handling Units Using Energy Feedback Control. *ASHRAE Trans.* **2022**, *128*, 59–66.
39. Wang, G.; Han, Z. Investigation of the accuracy of VFD analog output data and the energy performance of different voltage controls in a VFD-motor-belt-fan system. *Energy Build.* **2019**, *194*, 260–272. [[CrossRef](#)]

**Disclaimer/Publisher’s Note:** The statements, opinions and data contained in all publications are solely those of the individual author(s) and contributor(s) and not of MDPI and/or the editor(s). MDPI and/or the editor(s) disclaim responsibility for any injury to people or property resulting from any ideas, methods, instructions or products referred to in the content.